SLAC-PUB-3229
September 1983
(A)

CALCULATION OF POLARIZATION EFFECTS

ALEXANDER W. CHAO*
Stanford Linear Accelerator Center
Stanford University, Stanford, California 94305

1. Introduction

Basically there are two areas of accelerator applications that involve beam polarization. One is the acceleration of a polarized beam (most likely a proton beam) in a synchrotron. Another concerns polarized beams in an electron storage ring. In both areas, numerical techniques have been very useful.

2. Accelerating Polarized Beams in a Synchrotron

In a proton synchrotron, a polarized beam is injected and then accelerated with its polarization parallel to the guiding magnetic field. If particles see only the guiding field, then there will be no depolarization effects. But perturbing magnetic fields, such as the quadrupole magnetic fields seen by an off-axis particle, will cause the particle spin to deviate from the vertical direction $\hat{y}$. This spin deviation will then precess around $\hat{y}$ with a precession frequency $a\gamma f_{rev}$, where f_{rev} is the revolution frequency, γ is the Lorentz energy factor and a is a fundamental constant given by

$$a = \begin{cases} 1.793 & \text{proton} \\ 0.001160 & \text{electron} \end{cases} \tag{1}$$

The quantity

$$\nu = a\gamma \tag{2}$$

is called the spin tune.

If ν is close to ν_0 which satisfies a resonant condition

$$\nu_0 = n_x\nu_x + n_y\nu_y + n_s\nu_s + n \quad , \tag{3}$$

a small perturbing magnetic field will lead to a substantial deviation of the spin direction which then gives rise to depolarization. In Eq. (3), ν_x, ν_y and ν_s are the horizontal, vertical and synchrotron tunes of the orbital motion of the particles and n, n_x, n_y, n_s are integers.

The degree of this depolarization depends on the distance between ν from ν_0. The closer ν is to ν_0, the stronger is the depolarization. The width around ν_0 within which the polarization is reduced by $>50\%$ is defined to be the depolarization resonance width. It is designated by ϵ and it depends on the strength of the perturbing magnetic field.

The problem comes from the fact that the spin tune is proportional to the particle energy. As a result it varies as the beam is being accelerated and in doing so crosses resonances. We then need to calculate the amount of polarization lost due to each crossing. This is done by applying the Foissart-Stora equation[1]

$$P_{+\infty} = P_{-\infty}\left(2e^{-\pi\epsilon^2/2\alpha} - 1\right) \tag{4}$$

where α is the crossing speed of ν relative to ν_0, $P_{-\infty}$ and $P_{+\infty}$ are the beam polarizations before and after crossing, respectively.

---

*Work supported by the Department of Energy, contract DE-AC03-76SF00515.
Invited talk to the Europhysics Conference, Computing in Accelerator Design and Operation, Berlin, West Germany, 20-23 September 1983

According to Eq. (4), there are two ways to assure a small polarization loss.[2-5] We either quickly cross a weak resonance ($\epsilon^2/\alpha \ll 1$) or slowly cross a strong resonance ($\epsilon^2/\alpha \gg 1$). In the later case, the polarization will be flipped after crossing. Anything in between the two extreme cases ($\epsilon^2/\alpha \simeq 1$) will be harmful for polarization.

The resonance crossing speed α is a strightforward kinematic quantity given by

$$\alpha = \frac{1}{2\pi}(a\Delta\gamma - \Delta\nu_0) \tag{5}$$

where $\Delta\gamma$ and $\Delta\nu_0$ are the changes of γ and ν_0 per revolution during acceleration. Fast crossing speed can be obtained by fast acceleration rate $\Delta\gamma$. For resonances that involve the orbital tunes, it can also be obtained by jumping the orbital tunes as the beam is being accelerated through the resonance by using pulsed quadrupole magnets.

The quantity in Eq. (4) that remains to be calculated is the resonance width ϵ. This needs to be done for all depolarization resonances crossed by the spin tune during the acceleration process.

3. Calculation of the Depolarization Resonance Widths

The basic equations of motion — the Thomas-BMT equation[6] — for the spin $\vec{S}$ in a magnetic field is

$$\dot{\vec{S}} = \vec{\Omega} \times \vec{S} \tag{6}$$

where

$$\vec{\Omega} = \frac{e}{m\gamma c}\left[(1+a\gamma)\vec{B}_\perp + (1+a)\vec{B}_\parallel\right]$$

where $\vec{B}_\parallel$ and $\vec{B}_\perp$ are the magnetic field components parallel and perpendicular to the instantaneous direction of motion, respectively. Note that the spin motion depends on the orbital motion since it is the orbital motion that determines the magnetic field seen by the particle. This is one reason why the spin motion is more difficult to analize than the orbital motion. The depolarization resonance width, for example, can be calculated only after the orbital motion has been analized.

More quantitatively, ϵ is defined as the Fourier component of $\vec{\Omega}$ at the resonance frequency,[1,7,8] i.e.,

$$\epsilon = \frac{1}{2\pi c}(\hat{x} - i\,\hat{z}) \cdot \int_{\pi 0}^{2} e^{i\nu_0\theta}\ \vec{\Omega}\ (\theta)\ \rho(\theta) d\theta \tag{7}$$

where $\hat{x}$ and $\hat{z}$ are the horizontal and longitudinal unit vectors, $\rho(\theta)$ is the bending radius and θ is the accumulated bending angle that increases by 2π every revolution.

It turns out that the strongest depolarization resonances belong to the two families[7-10]

$$\nu = n \ : \text{imperfection resonances excited by vertical closed orbit distortion;} \tag{8a}$$

$$\nu = nS \pm \nu_y \ : \text{intrinsic resonances excited by vertical betatron motion of particles } (S \text{ is the periodicity of the accelerator.}) \tag{8b}$$

For these resonances, we need only to keep in $\vec{\Omega}$ those terms linear in the orbital coordinates.[8] When this is done, Eq. (7) becomes

$$\epsilon \approx \frac{1+a\gamma}{2\pi}\int_0^{2\pi} G(\theta)\, y(\theta)\, e^{i\nu_0\theta}\, \rho(\theta)\, d\theta \tag{9}$$

where G is the quadrupole strength. From Eq. (9), we see that most of the depolarization action results from having vertical excursion in quadrupoles. In deriving Eq. (9), we have assumed that the accelerator has a planar geometry by design and there is no solenoidal field.

The widths of the imperfection resonances are obtained by setting y=closed orbit distortion in Eq. (9). To do a calculation, it is necessary to input a Monte Carlo simulation of the closed orbit error with a certain given rms. The intrinsic resonance widths on the other hand are obtained by setting =betatron excursion in Eq. (9) and do not require any random number generations. Their strengths are calculated once the accelerator lattice is determined and the beam emittance is known.

Table 1 shows the number of imperfection and intrinsic resonances that the polarized proton beam has to cross for several accelerators. Obviously the high energy synchrotrons will have more resonances to cross than the lower energy ones.

Table 2 shows the intrinsic resonance widths[7] for three synchrotrons using the program DEPOL.[8] The results are for particles whose emittance is the average beam emittance. Resonance widths have also been calculated for ZGS,[9] KEK-PS[4] and SATURNE.[3]

4. Acceleration to High energies

To accelerate polarized proton beams to very high energies requires special effort. This is first of all due to the fact that the total number of resonances to be crossed is simply very large. (See Table 1.) Secondly, high energy synchrotrons typically have strong focussing lattices which tend to give stronger resonances than the weak focussing lattices. Thirdly, resonance widths tend to increase as energy goes higher.

Somewhat more quantitatively, let us take the resonance widths to be very roughly[11]

$$\begin{aligned} \epsilon_{\rm int} &\approx 0.02(E/25\ \text{GeV})^{1/2} \\ \epsilon_{\rm imp} &\approx 3\times 10^{-4}(E/25\ \text{GeV}) \end{aligned} \tag{10}$$

The imperfection resonance width is meant to be that after an orbit correction has been applied. If we then take the fast crossing approach, the total loss of polarization after crossing all resonances is

$$\frac{\Delta P}{P} \approx \sum_{i=\rm int} \frac{\pi\epsilon_i^2}{\alpha_{\rm int}} + \sum_{i=\rm imp} \frac{\pi\epsilon_i^2}{\alpha_{\rm imp}} \tag{11}$$

If we assume that the acceleration speed is determined by a given rf acceleration per unit distance while the ν_y-jump is determined by jumping ν_y by 0.2 in 1 μsec, then the resonance crossing speeds scale like

$$\begin{aligned} \alpha_{\rm int} &\approx 0.05(\hat{E}/25\ \text{GeV}) \\ \alpha_{\rm imp} &\approx 5\times 10^{-5}(\hat{E}/25\ \text{GeV}) \end{aligned} \tag{12}$$

where $\hat{E}$ is the maximum energy of the synchrotron. Note that part of the increase in resonance widths with energy is compensated by the increase in crossing speed for higher energy synchrotrons.

Substituting Eqs. (10) and (12) into Eq. (11) and assuming a periodicity of $S = 8$, we obtain

$$\frac{\Delta P}{P} \approx 6\times 10^{-3}\,E(\text{GeV}) + 1.5\times 10^{-4}\,E(\text{GeV})^2 \tag{13}$$

Note that for very high energy synchrotrons, the imperfection resonances dominate the depolarization.[12] If we demand $\Delta P/P < 50\%$, the maximum energy that a polarized proton beam can be accelerated to is then found to be about 40 GeV, which is not too much beyond the AGS energy.

Table 1

Accelerator	Energy (GeV)	Number of Intrinsic Resonances	Number of Imperfection Resonances
ZGS	12	10	22
SATURNE	3	2	6
FNAL (booster)	8	1	14
KEK-PS	12	10	21
AGS	30	9	56
CERN-PS	30	12	55
CERN-ISR	11.5-31.4	10	38
FNAL (main ring)	8-400	250	749
SPS	10-400	249	745
FNAL (Tevatron I)	150-1000	541	1626

Table 2

CERN-PS			AGS			FERMILAB (main ring)*		
ν	γ	$\lvert\epsilon\rvert$	ν	γ	$\lvert\epsilon\rvert$	ν	γ	$\lvert\epsilon\rvert$
$10-\nu_y$	2.06	.00005	$12-\nu_y$	1.82	.0054	$0+\nu_y$	10.84	.0256
$0+\nu_y$	3.53	.00933	$0+\nu_y$	4.89	.01535	$6+\nu_y$	14.19	.0060
$20-\nu_y$	7.64	.00045	$24-\nu_y$	8.52	.00059	$12+\nu_y$	17.54	.0035
$10+\nu_y$	9.12	.00047	$12+\nu_y$	11.59	.00539	$18+\nu_y$	20.89	.0016
$30-\nu_y$	13.23	.00087	$36-\nu_y$	15.22	.01373	$24+\nu_y$	24.25	.0025
$20+\nu_y$	14.70	.00050	$24+\nu_y$	18.29	.00101	$30+\nu_y$	27.60	.0049
$40-\nu_y$	18.82	.00077	$48-\nu_y$	21.93	.00148	$36+\nu_y$	30.95	.0062
$30+\nu_y$	20.29	.00309	$36+\nu_y$	25.00	.02663	$42+\nu_y$	34.30	.0057
$50-\nu_y$	24.40	.14192	$60-\nu_y$	28.63	.15666	$48+\nu_y$	37.65	.0028
$40+\nu_y$	25.88	.00174	$48+\nu_y$	31.70	.00233	$54+\nu_y$	41.01	.0021
$60-\nu_y$	29.99	.00195				$60+\nu_y$	44.36	.0048
$50+\nu_y$	31.64	.16773				$66+\nu_y$	47.71	.0098
						$72+\nu_y$	51.06	.0133
						$78+\nu_y$	54.41	.0198
						$84+\nu_y$	57.77	.0321
						$90+\nu_y$	61.12	.0518
						$96+\nu_y$	64.47	.1653
						$192+\nu_y$	118.10	.0560
						$288+\nu_y$	171.73	.2952
						$384+\nu_y$	225.36	.0921
						$480+\nu_y$	278.99	.2138
						$576+\nu_y$	332.63	.0998
						$672+\nu_y$	386.26	.2995
						$768+\nu_y$	439.89	.0244

*Only dominant ones.

In view of this, a better way of acceleration to high energies is needed. One such possibility is called harmonic matching. Another is to install Siberian snake devices in the accelerator. These two topics are discussed in the following two sections.

5. Harmonic Matching

The idea of harmonic matching is to make $\epsilon = 0$ at the moment of crossing a resonance so that there will be no loss of polarization due to the crossing. For the imperfection resonances, the condition for achieving this is given by[13] (cf. Eq. (9))

$$\frac{1}{2\pi}\int_0^{2\pi} \exp(i\nu_0\theta)\, d\theta\; G(\theta) y_{co}(\theta) = 0 \tag{14}$$

where $y_{c.o.}$ is the vertical closed orbit distortion. Equation (14) is a Fourier harmonic of the vertical closed orbit, thus the name harmonic matching. Since (14) is a complex quantity, it imposes two conditions on $y_{c.o.}$ for each resonance to be crossed.

Before applying (14), there needs to be a good orbit correction in the rms manner. The orbit is then slightly changed to fulfill (14). The amount of change is rather small and is obtained not by the beam position monitor measurements but by empirically optimizing the polarization.

Harmonic matching for the imperfection resonances has been used successfully in ZGS and SATURNE. On-line controls have been applied so that a vertical orbit distortion with the right harmonics is generated shortly before crossing and switched off shortly after crossing the resonance. The control program makes orbit distortions in symphony with the acceleration process.

To accelerate polarized protons in high energy synchrtrons using the harmonic matching technique, however, one needs to do a more accurate matching than ZGS and SATURNE so that the imperfection resonance widths are much narrower than Eq. (10) gives.

To harmonic match the intrinsic resonances is more difficult. The quantity to be matched is[14]

$$\frac{1}{2\pi}\int_0^{2\pi} \exp\Big[i(\nu_0\theta - \psi_y(\theta))\Big]\, d\theta\; G(\theta)\sqrt{\beta_y(\theta)} = 0 \tag{15}$$

where ψ_y and β_y are the vertical betatron phase and beta-function, respectively.

At the moment of crossing, the quadrupole strengths are changed to satisfy (15). To minimize the effect on the betatron motions, this may have to be done keeping the tunes constant during the crossing process. Note that the quadrupole strengths are calculated by a lattice fitting routine rather than found empirically.

So far harmonic matching for intrinsic resonances has not been applied to existing synchrotrons. It is conceivable, however, that some intrinsic resonances (in the smaller synchrotrons for which Siberian snakes are not applicable) can be crossed this way.

6. Siberian Snakes

A Siberian snake[15] is a series of horizontal and vertical bending magnets that does two things:

1. Makes spin tune ν equal to 1/2, and
2. Does not affect the beam orbit outside the device.

A Siberian snake therefore makes the spin tune independent of the beam energy and thus eliminates the need to cross resonances.

There are two types of snakes:

Type I rotates the polarization by 180° around the longitudinal $\hat{z}$-axis, and

Type II rotates the polarization by 180° around the horizontal $\hat{x}$-axis.

One way to use the snake is to insert a type I snake at a symmetry point in the synchrotron. Another way is to have a type I snake at a symmetry point and another type II snake at the opposite symmetry point. The spin tune in both cases will be 1/2.

There are several possible designs of Siberian snakes. An explicit example of a type I snake is[16]

$$\begin{array}{ccccccccc} V & H & V & H & V & H & V & H & V \\ (45) & (45) & (-90) & (-90) & (90) & (90) & (-90) & (-45) & (45) \end{array} \tag{16}$$

where H and V mean horizontal and vertical bending magnets and the quantities in parentheses are the spin precession angles in degrees.

An explicit example of a type II snake is[16]

$$\begin{array}{ccccccc} V & H & V & H & V & H & V \\ (-90) & (90) & (90) & (-180) & (90) & (90) & (-90) \end{array} \tag{17}$$

To make spin to precess by fixed angles like the snake magnets do, the magnet strengths have to be independent of beam energy even during acceleration. One consequence of this is on the beam-stay-clear requirements. Although there is no net effect on the beam trajectory outside of the snake, the orbit distortion in the snake is not negligible, especially at the lower energies. (For this reason, Siberian snakes are not applicable to synchrotrons of low injection energy.) This beam-stay-clear requirement imposes strong constraints on the snake aperture and is a major concern facing the snake designers.

Error effects with snakes also need attention. Some analytical work has been performed,[17] which concludes that if a resonance existed before inserting the snake, then it may still have a remnant depolarization effect after the snake is inserted. In particular, if the accelerator has a resonance width ϵ in the absence of the snake, and if the two circular arcs of the accelerator contribute equally to the resonance width, then after the snake is inserted the resonance will shift the spin tune away from 1/2 according to[17,11]

$$\begin{aligned} \text{single snake} &: \nu = \frac{1}{2} + |\epsilon| \cos\phi \\ \text{double snake} &: \cos \pi\nu = \cos 2\phi \, \sin^2(\pi|\epsilon|/2) \end{aligned} \tag{18}$$

where ϕ is the phase factor of the complex resonance width. Clearly if the spin tune is shifted to a value that satisfies a resonant condition, then even the great snakes do not save the polarization. Numerical simulation of errors and tracking the spin motion crossing resonances in the presence of a snake will yield useful information here.

7. More studies

In this section, we mention a few additional effects that can be studied by numerical means.

(1) The imperfection and the intrinsic resonances are not the only ones encountered during acceleration. The other resonances, although weaker, can still contribute to loss of polarization. Among them are

$$\nu = n \pm \nu_y \text{ : excited by quadrupole field errors that destroy the periodicity} \tag{8c}$$
$$\nu = n \pm \nu_x \text{ : excited by horizontal excursion in skew quadrupoles} \tag{8d}$$
$$\nu = nS \pm \nu_x \pm \nu_y \text{ : excited by sextupoles} \tag{8e}$$

Furthermore, multipole field errors will excite higher order resonances. Widths of these resonances need to be calculated. The programs that are used to calculate the imperfection and intrinsic resonances can be extended easily to calculate for resonances of type (8c) but not for types (8d) and (8e).

It should be pointed out that Eq. (9) is a result after linearization. To calculate the width of a nonlinear resonance, the more general result, Eq. (7), must be used in which nonlinear terms up to the proper order are included in $\vec{\Omega}$. One step toward this direction has been made in Ref. 18; the spin rotations are calculated to second order for quadrupoles and for sextupoles.

(2) The Froissart-Stora equation assumes a single isolated depolarization resonance. This assumption is not valid if the synchrotron oscillation plays a role during the resonance crossing.

According to the F-S equation, the polarization after crossing versus the resonance strength is a simple exponential function given by Eq. (4). What was observed in SATURNE for the imperfection resonance $\nu = 2$, however, looks like Fig. 1(a).[3] The discrepancy has been recently explained by the SATURNE group[19] using a tracking simulation taking into account of synchrotron oscillations. Part of their results is shown in Fig. 1(b). The agreement is rather convincing.

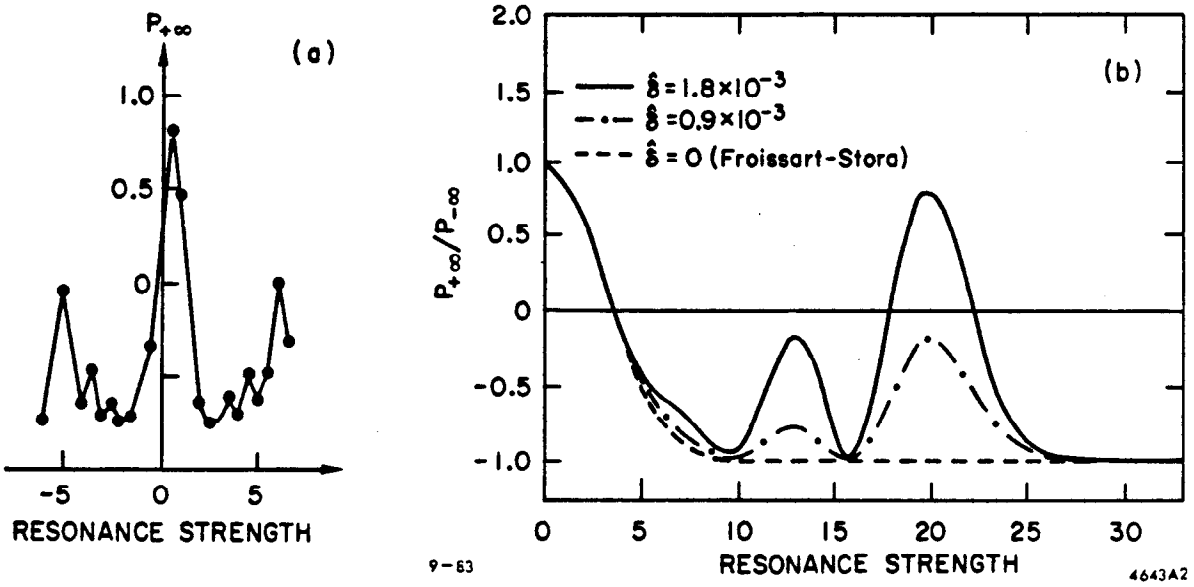

Fig.1. (a) measured polarization after crossing the $\nu = 2$ resonance in SATURNE versus the resonance strength which is controlled by exciting a vertical orbit distortion. (b) result of a simulation taking into account of synchrotron oscillations.

(3) In performing a slow crossing of an intrinsic resonance, particles with small emittance may not get flipped since their resonance widths are narrow. Simulation may help in estimating polarization loss due to this effect.

(4) Crossing is not necessarily done with a uniform speed from $\nu - \nu_0 = -\infty$ to $+\infty$. For instance, when crossing an intrinsic resonance, the crossing speed may be temporarily much enhanced by a ν_y-jump. This makes the Froissart-Stora equation not applicable.

Equivalents of the $F-S$ equation exist for a few special cases of crossing scheme.[8,20] However, one might still need to consider complicated crossing schemes in practice. One reason is that the pulsed quadrupoles generally have complicated time response. Another reason (perhaps minor) is that the crossing speed assumed in the $F-S$ equation is uniform in the variable θ (the accumulated bending angle), while in practice the energy accelerations are made at the rf cavities. Numerical tracking will of course be useful for general crossing schemes.

(5) When crossing an intrinsic resonance with a ν_y-jump, the pulsed quadrupoles alters the accelerator focussing lattice. Effects of this on the orbital motions – and thus on the depolarization resonance width — should be studied.

8. Polarization in an Electron Storage Ring

In a proton synchrotron, the main problem is to accelerate a beam crossing depolarization resonances. In an electron storage ring, we have a different problem. The beam energy is constant in time and depolarization comes from the noise associated with synchrotron radiation.

Another difference between protons and electrons is that a stored electron beam will slowly polarize itself through the Sokolov-Ternov mechanism.[21] If an unpolarized beam is injected into a storage ring, its polarization will build up exponentially along the vertical $\hat{y}$ direction according to

$$P(t) = \frac{P_0}{1+x}\left[1 - \exp\left(-\frac{(1+x)}{\tau_P}\, t\right)\right]$$
$$x = \frac{\tau_P}{\tau_D} \tag{19}$$

where $P_0 = 8/5\sqrt{3} = 92\%$ is the polarization level reachable in the absence of depolarization effects, τ_P is the polarization time constant given by

$$\tau_P = 99 \text{ sec } \frac{R(m)\,\rho(m)^2}{E(\text{GeV})^5} \tag{20}$$

with R the average ring radius and ρ the bending radius.

The depolarization effects are lumped into the parameter τ_D. In a planar ring without errors, there is no depolarization effects and $\tau_D = \infty$. Otherwise τ_D needs to be calculated. In the next two sections, we will describe a program SLIM that offers such a calculation.

9. SLIM Without Spin[22]

Before going on to discuss the polarization calculations, we will first describe the part of SLIM that calculates the orbital quantities regardless of spin since the technique used here is different from the conventional method and will be useful in describing the spin calculations later.

We begin with the vector[23]

$$X = \begin{bmatrix} x \\ x' \\ y \\ y' \\ z \\ \Delta E/E \end{bmatrix} = \begin{bmatrix} x_1 \\ x_2 \\ x_3 \\ x_4 \\ x_5 \\ x_6 \end{bmatrix} \tag{21}$$

that describes the orbital deviations of an electron. All beam-line elements (bends, quads, rf cavities, skew quads, solenoids and drifts) are then described by 6×6 matrices. Sextupoles are included by linearization around the closed-orbit.

The most distinct feature of SLIM is that it employs an eigen-analysis and all interested physical quantities are expressed in terms of the eigenvalues and eigenvectors resulting from the analysis. This is in contrast to the conventional technique which expresses the physical quantities in terms of the various machine functions (the β-functions and phases, the dispersion functions, etc). The adavantage is that by using a 6×6 formalism, all coupling effects among the three dimensions are included. As a comparison, the β-functions are undefined when there is x-y coupling. This advantage becomes critical when performing the polarization calculations because spin motion depends sensitively on the orbital motions and it is necessary to include the spin-orbit couplings between spin and all three orbital degrees of freedom.

Once the storage ring lattice — including the quadrupole misalignments and orbit correctors — is determined, a closed-orbit is calculated in the 6-dimensional phase space.

As shown in Fig.2, there are two places (indicated by dotted boxes) where SLIM makes detours to calculate the unperturbed and the perturbed machine functions. These are for display only and not used later.

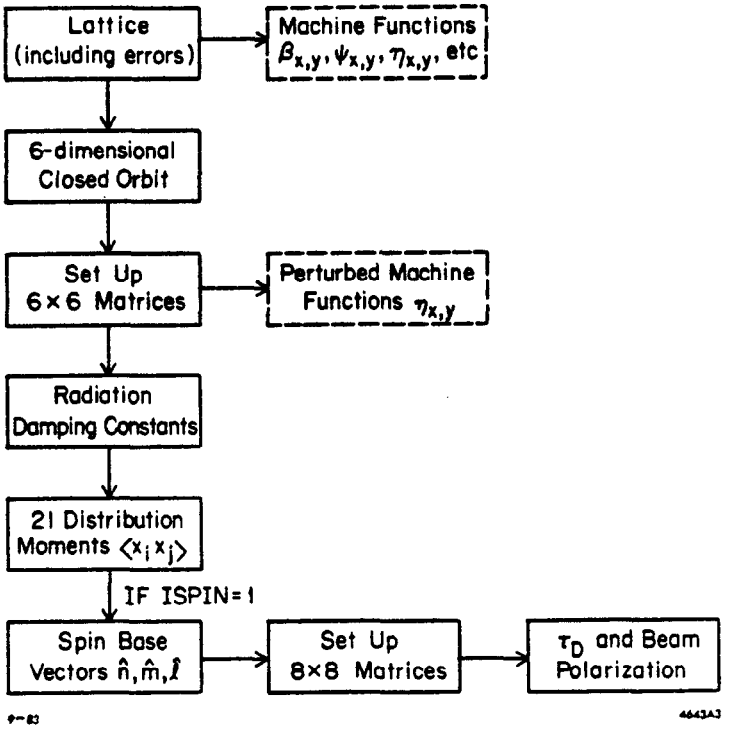

Fig. 2. Flow chart for SLIM.

Knowing the matrices of all the beam-line elements, we multiply them sequentially to obtain a total 6×6 matrix. The eigenvalues of this total matrix form three complex conjugate pairs. If the linear lattice is stable, all eigenvalues have absolute value of unity. Otherwise the motion is unstable and the program is stopped. The eigenvalues then give the three tunes according to

$$\lambda_k = \exp(\pm i 2\pi\nu_k) \qquad k = \mathrm{I},\ \mathrm{II}, \mathrm{III} \tag{22}$$

Radiation damping constants are calculated by slightly modifying the 6×6 matrices. For example, the rf cavity matrix will take into account of the reduction in x' and y' due to the acceleration by changing the 22- and the 44-elements from 1 to 1-eV/E. The bending magnets and the quadrupoles will also be similarly modified. After these modifications, we multiply matrices to obtain a total 6×6 matrix whose determinant is no longer unity. The eigenvalues of this matrix then give the radiation damping constants α_k:

$$\lambda_k = \exp(-\alpha_k \pm i 2\pi\nu_k) \qquad k = \mathrm{I},\ \mathrm{II},\ \mathrm{III} \tag{23}$$

The beam is stable if all three damping constants are positive. Otherwise, the program is terminated.

The program also gives the beam distribution in the 6-dimensional phase space by calculating the second moments:

$$\langle x_i x_j \rangle(s) = 2 \sum_{k=\mathrm{I,II,III}} \langle |A_k|^2 \rangle \ \mathrm{Re}\ [E_{ki}(s) E^*_{kj}(s)] \tag{24}$$

with

$$\langle |A_k|^2 \rangle = 7.2 \times 10^{-28} \frac{\gamma^5}{\alpha_k} \oint ds \frac{|E_{k5}(s)|^2}{|\rho(s)|^3}$$

where $E_k(s)$ is the k-th eigenvector (complex) of the 6×6 matrix for one revolution around s and E_{ki} is the i-th component of E_k. We have assumed that the eigenvectors have been normalized and all lengths are expressed in meters. Eq.(24) of course contains information on the x- and y-emittances, bunch length, beam energy spread, tilting angles in $x-x'$, $y-y'$, $x-y$ planes, etc.

If the flag command for doing the spin calculations is on, we then proceed to the next section.

10. SLIM with Spin[24,25]

Knowing the electric and magnetic fields along the closed orbit, spin motion of a particle that follows the closed orbit can be determined by the Thomas-BMT equation. Each beam-line element is then associated a 3×3 rotation matrix that describe the spin precession in this element. Multiplying all these 3×3 matrices together gives a total rotation matrix T.

The beam polarization at equilibrium is going to lie along a direction $\hat{n}(s)$ at position s. It is given by the rotational axis of the rotation T, i.e.

$$T\hat{n} = \hat{n} \tag{25}$$

A fully polarized particle will have its spin along $\hat{n}$. Two axiliary unit vectors $\hat{m}$ and $\hat{\ell}$ are then defined so that $\hat{n}$, $\hat{m}$, and $\hat{\ell}$ form an orthogonal set and precess according to the Thomas-BMT precession along the closed orbit. In general, a slightly depolarized electron will have spin

$$\vec{S} = \hat{n} + \alpha\hat{m} + \beta\hat{\ell} \tag{26}$$

where $|\alpha, \beta| \ll 1$.

The spin part of SLIM is a generalization of the orbital part. The difference is that the spin degree of freedom is included in addition to the three orbital degrees of freedom. The vector instead of (21) is now

$$X = \begin{bmatrix} x \\ x' \\ y \\ y' \\ z \\ \Delta E/E \\ \alpha \\ \beta \end{bmatrix} \tag{27}$$

The next step is to form the corresponding 8×8 matrices for all beam-line elements that transform the vector (27). The upper-left corner of these matrices will be simply the 6×6 matrices used in the orbital calculations. The upper right 6×2 will be zero because spin motion does not affect orbital motions. The lower-right 2×2 gives the spin precession while the lower-left 2×6 gives the critical spin-orbit coupling coefficients. The matrix looks like

$$\left[\begin{array}{c|c} \text{TRANSPORT} & 0 \\ \hline \begin{array}{c}\text{spin-orbit} \\ \text{coupling}\end{array} & \begin{array}{c}\text{spin} \\ \text{precession}\end{array} \end{array}\right] \tag{28}$$

We then multiply all 8×8 matrices in sequence to obtain the total matrix and calculate its eigenvalues and eigenvectors. Three pairs of the eigenvalues and eigenvectors are the orbital ones.

obtained before. The fourth eigenvalue gives the spin precession tune, while the fourth eigenvector is used to calculate τ_D *

$$\tau_D^{-1}(\sec^{-1}) = 8.64 \times 10^{-19} \frac{\gamma^5}{C} \oint \frac{ds}{|\rho(s)|^3} \left[\left(\mathrm{Im} \sum_k E_{k5}^* E_{k7} \right)^2 + \left(\mathrm{Im} \sum_k E_{k5}^* E_{k8} \right)^2 \right]_s \quad (29)$$

where C is the circumference of the ring. Eq. (29) is the final result. The procedure of spin calculation is illustrated in Fig. 2.

To simulate the depolarization effects, we start with a perturbed lattice with a known distribution of orbit distortion dipoles representing quadrupole misalignments. The resulting orbit distortion is then corrected by a set of orbit correctors to an rms value similar to that observed. Such a distorted lattice, including sextupoles, are fed into SLIM to calculate the equilibrium polarization, $P_0/(1+x)$ of Eq. (19). The results are typically plotted while scanning the beam energy.

If the beam energy is such that the spin tune $\nu = a\gamma$ is close to one of the linear depolarization resonances

$$\nu \pm \nu_{x,y,s} = n \quad (30)$$

SLIM predicts a strong spin-orbit coupling and thus a loss of beam polarization. Due to the matrix technique used, SLIM does not give any information on the nonlinear resonances.

Figure 3 is the result of a simulation for the storage ring SPEAR. The rms orbit after correction is 1.2 mm. Figure 3 also shows the experimental results.[26] As can be seen, the agreement is satisfactory except that the nonlinear resonance $\nu - \nu_x + \nu_s = 3$ has been missed by the simulation.

It should be emphasized that the orbit distortion in the simulation is the one after correction. The Fourier contents of a corrected orbit and an uncorrected orbit are very different – yielding very different predictions on polarization – even if the two have the same rms value. See Fig. 4.

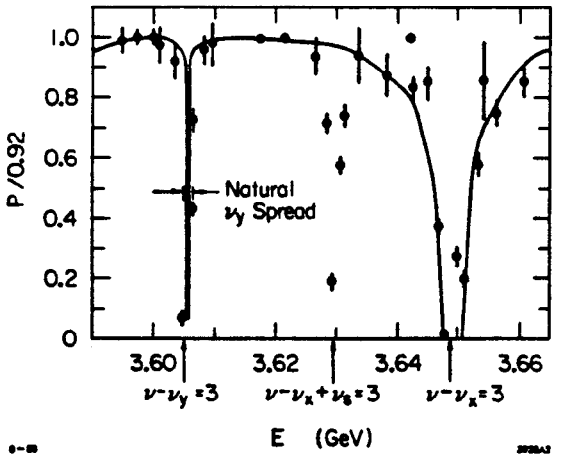

Fig. 3. SLIM simulation compared with the measured data for the storage ring SPEAR.

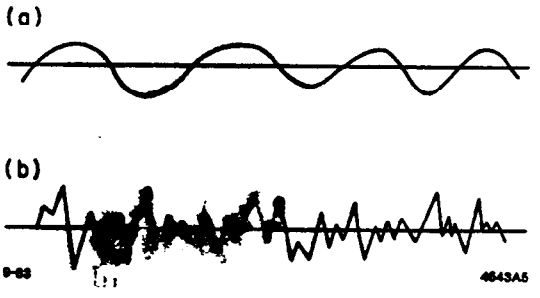

Fig. 4. (a) orbit before correction; (b) orbit after correction.

* More accurately what is calculated is the so-called spin-orbit coupling vector, or equivalently the spin chromaticity. Such details are omitted in this work.

Clearly calculations of ϵ for a proton synchrotron and τ_D for an electron storage ring are closely related. It has not been demonstrated explicitly how this can be done and how programs can be applied to both cases. If this is established, then for instance the eigen-analysis can be applied to proton synchrotrons as well and vise versa for the proton programs.

11. Nonlinear Effects

As mentioned before, one serious drawback of the SLIM technique is that it does not treat the nonlinear resonances. These include the sextupole resonances (8e) and the synchrotron sideband resonances $\nu \pm \nu_{x,y} \pm k\nu_s = n$ with $k \neq 0$. These resonances have been observed in SPEAR[26] and will only be stronger for the higher energy rings because

— the sextupoles tend to be stronger, and

— the energy spread is larger and synchrotron motion becomes important

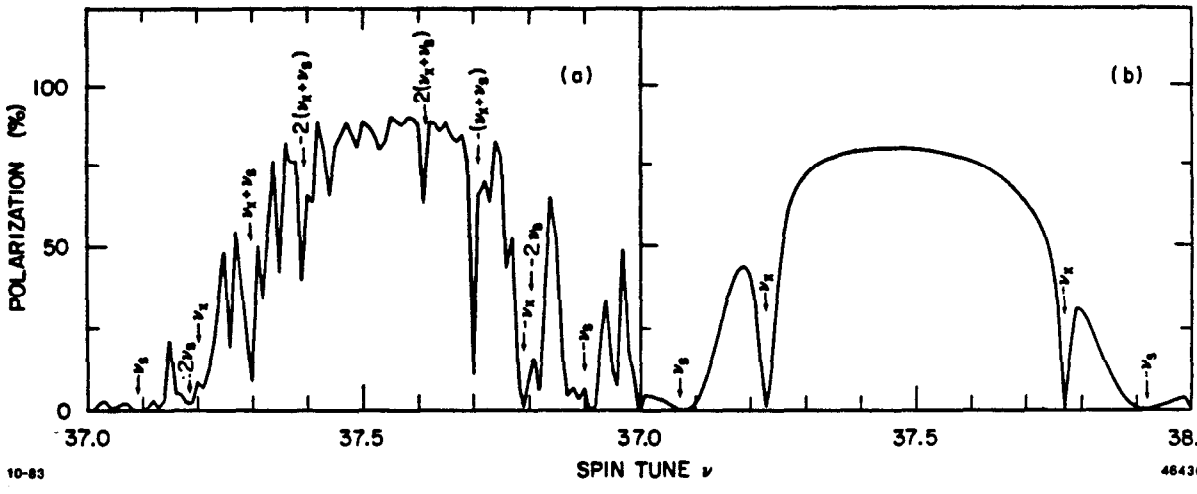

Fig. 5. (a) results of SITROS tracking for the storage ring PETRA;
(b) SLIM results for the same lattice.

One effective way of studying the nonlinear effects is by numerical simulations, as done by Kewisch using the program SITROS.[27] The result for the storage ring PETRA is shown in Fig.5(a). It clearly contains a structure of nonlinear depolarization resonances. Fig.5(b) gives the linear SLIM calculation for the same lattice. There is a general qualitative agreement between these results.

A simulation program can also be used to study the effect of beam instabilities on polarization. One might expect that if the beam intensity becomes high enough so there is a significant blow-up of the beam emittance, the effect on polarization will not be negligible.

One more possible application of a tracking program is to simulate the spin motion when two beams collide. The beam-beam interaction is a very nonlinear effect, potentially exciting depolarization resonances of high orders.[28] In this respect, there has been suggestions[29,30] of imposing a special set of spin matching conditions (see next section) exclusively for the beam-beam interaction. One such suggestion[30] is based on the argument that, although higher order resonances are excited, beam-beam depolarization is dominated by the linear $\nu \pm \nu_y = n$ resonance with the higher order resonances smaller by a factor of the order of τ_{rad}/τ_P (where τ_{rad} is the radiation damping time) which is $\ll 1$. If such a beam-beam spin matching can indeed be achieved, the beam-beam interaction will no longer cause depolarization. These expectations need to be confirmed by a large amount of tracking efforts.

12. Longitudinal Polarization and Spin Matching

Up to now, we have been talking about a vertical beam polarization. The experimenters, however, may request for a longitudinal polarization at the interaction points (IP) where beams collide. To do that, we install a "spin rotator" which consists of a few horizontal and vertical bending magnets on one side of the IP to rotate the polaeizarion from $\hat{y}$ to $\hat{z}$-direction and similarly on the other side of the IP to restore the polarization from $\hat{z}$- back to $\hat{y}$-direction. In the rest of the ring, polarization is along $\hat{y}$.

One design of spin rotator is the "mini-rotator" for HERA.[31] On one side of the IP, the rotator consists of

$$\text{arc} \leftarrow \underset{(-38.925)}{V} \quad \underset{(-62.3)}{H} \quad \underset{(77.85)}{V} \quad \underset{(90)}{H} \quad \underset{(-38.925)}{V} \quad \underset{(44.353)}{H} \rightarrow \text{IP} \tag{31}$$

On the other side, the H magnets are symmetric with respect to the IP while the V magnets are anti-symmetric. The total length of the section (31) is 45.5 m. The H magnets are part of the normal bending in the ring geometry. There are no quadrupoles in the insertion.

Fig. 6 shows the lattice and beam envelopes for HERA with mini-rotator. A typical problem for the spin rotator designs is the orbit distortion inside of the rotator (just like for the Siberian snakes) and the associated stringent beam-stay-clear requirements. The mini-rotator has a 17 cm maximum vertical orbit displacement at 27.5 GeV and varies with the beam energy.

There is another more subtle problem: rotators are very strong depolarizing devices. To avoid their depolarization effects, it is necessary to fulfill a set of conditions on the quadrupole distribution of the ring called the spin matching conditions.[32] The exact number of these conditions vary with details of the rotator design. Typically there are 10 conditions with several of them automatically satisfied due to symmetry of the lattice.

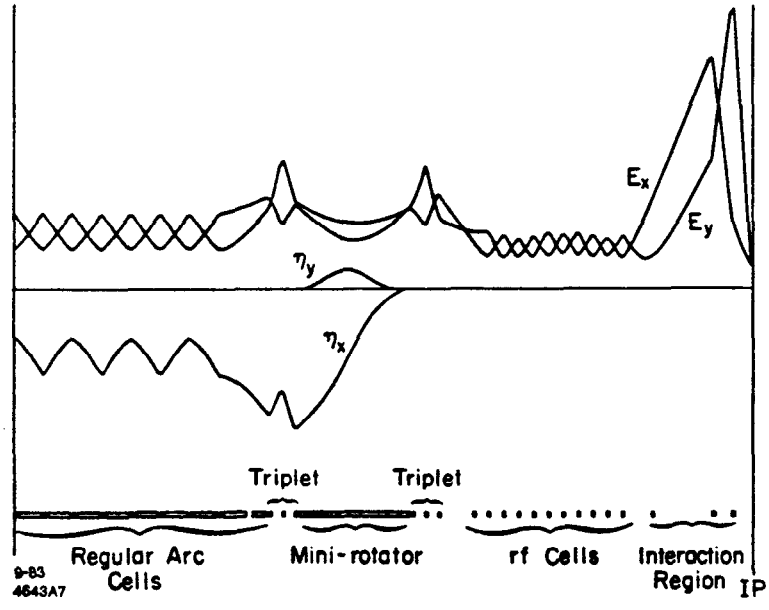

Fig. 6. HERA lattice with the mini-rotator.

For the mini-rotator, there are 4 nontrivial spin matching conditions to fulfill.[31] Two of them are imposed on the regular arc sections:

$$\int_{\text{arc}} G\sqrt{\beta_y}\, \cos\psi_{\text{spin}}\, \cos\psi_y\, ds = 0$$
$$\int_{\text{arc}} G\sqrt{\beta_y}\, \sin\psi_{\text{spin}}\, \sin\psi_y\, ds = 0 \tag{32}$$

where ψ_{spin} and ψ_y are the spin precession phase and the vertical betatron phase defined to be zero at the midpoint of the arc. The other two conditions are for the interaction region:

$$\int_{\text{I.R.}} G\sqrt{\beta_x}\,\cos\psi_x\,ds = 0$$
$$\int_{\text{I.R.}} G\sqrt{\beta_y}\,\cos\psi_y\,ds = 0 \qquad (33)$$

where $\psi_{x,y}$ are set to zero at the IP.

A fitting program is needed to simultaneously perform the optical and spin matchings. For the mini-rotator, quadrupole strengths in the interaction region and in the arc are used as fitting variables. Such a fitting program eventually will become part of the on-line lattice control program.

13. Imperfections and Harmonic Matching

Depolarization resonances are excited by imperfections. It turns out that for each resonance, there exist two conditions that would eliminate its strength. (This is similar to the proton synchrotron case, remember that ϵ is a complex quantity and to make $\epsilon = 0$ requires two conditions.) In PETRA, the beam polarization has been shown to improve from 30% to 80% by varying a certain Fourier components of the vertical closed orbit.[13] Such a procedure is called harmonic matching. The change in orbit to reach the best polarization is hardly noticeable. These effects have been simulated on SLIM, yielding Fig.7.[33]

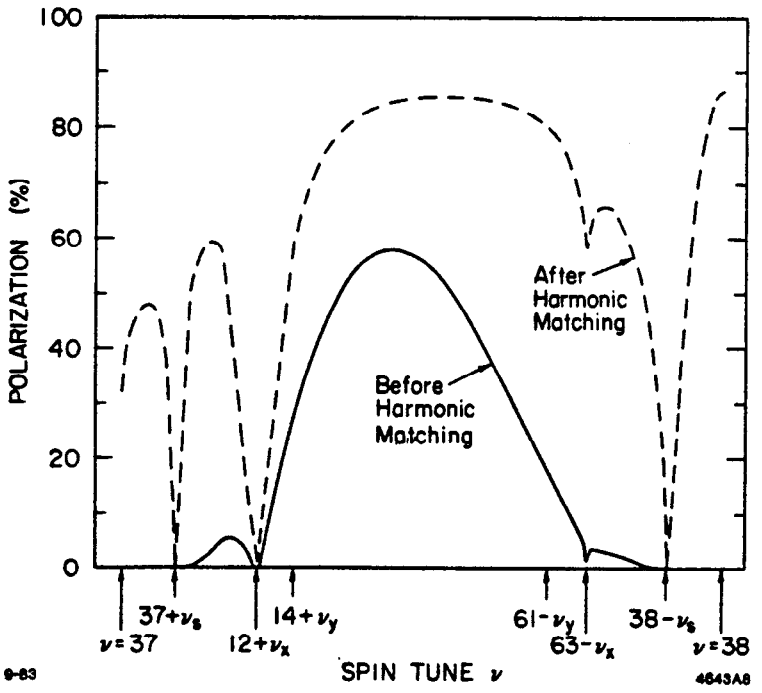

Fig. 7. Simulation of improving beam polarization by harmonic matching.

The spin matching and harmonic matching described above are linear effects. Strong nonlinearities may contaminate these matchings and cause depolarization. This is especially a question for the higher energy storage rings such as LEP, as explained before. A tracking program would provide useful information here.

Each depolarization resonance caused by imperfections requires two knobs for harmonic matching. The number of nearby resonances then determines the total number of knobs needed to optimize the polarization. Since the spin matching and the harmonic matching are both based on

the principle of eliminating the resonance strengths, it is conceivable that some of the harmonic matching knobs can be conveniently provided by the quadupoles that are used to spin match the rotators. The right hand side of eqs.(32) and (33) are then replaced by values that an operator desires to tweak into the storage ring.

Acknowledgement

I would like to thank J. Laclare, E. Grorud, D. Barber, H. Mais, W. Bialowons, G. Ripken and J. Kewisch for providing me very useful information. Barber, Mais and Ripken also pointed out a mistake of mine in the oral report of this work.

References

1. M. Froissart and R. Stora, Nucl. Inst. Methods, 7, 297 (1960).
2. T. Cho et al., Conf. High Energy Physics with Polarized Beams and Polarized Targets, AIP Proc. No. 35, Argonne, 1976, page 396.
3. E. Grorud et al., Conf. High Energy Spin Physics, AIP Proc. No. 95, Brookhaven, 1982, page 407.
4. S. Hiramatsu and K. Muto, Conf. High Energy Physics with Polarized Beams and Polarized Targets, Lausanne, 1980, Experientia Supplementum, Vol. 38, page 475.
5. L. G. Ratner, Ref. 3, page 412.
6. V. Bargmann, L. Michel and V. L. Telegdi, Phys. Rev. Lett. 2, 435 (1959).
7. L. Teng, Conf. High Energy Physics with Polarized Beams and Polarized Targets, AIP Proc. No. 51, Argonne, 1978, page 248.
8. E. D. Courant and R. D. Ruth, Brookhaven Report BNL-51270 (1980).
9. T. Khoe et al., Part. Accel. 6, 213 (1975).
10. E. Grorud, J. L. Laclare and G. Leleux, IEEE Trans. Nucl. Sci., NS-26, 3209 (1979).
11. R. Ruth, 12th Int. Conf. High Energy Accel., Chicago, 1983.
12. E. D. Courant, Conf. High Energy Spin Physics, AIP Proc. No. 95, Brookhaven, 1982, page 388.
13. H. D. Bremer et al., Ref. 3, page 400.
14. A. W. Chao, Ref. 3, page 458.
15. Ya. S. Derbenev and A. M. Kondratenko, Proc. 10th Int. Conf. High Energy Accel.,Protvino, 1977, Vol.2, page 70.
16. K. Steffen, DESY Report 83-058 (1983).
17. E. D. Courant, Ref. 4, page 102.
18. D. Carey, Ref. 3, page 454.
19. J. Laclare, E. Grorud, private communications (1983).
20. A. Turrin, IEEE Trans. Nucl. Sci., NS-26, 3212 (1979). Also, A. Turrin, Ref. 3, page 461.
21. A. A. Sokolov and I. M. Ternov, Sov. Phys. Dokl. 8, 1203 (1964).
22. A. W. Chao, J. Appl. Phys., 50, 595 (1979).
23. A similar technique has been used in A. Garren and A. S. Kenny, SYNCH program.
24. A. W. Chao, Nucl. Instr. Methods 180, 29 (1981).
25. H. Mais and G. Ripken, DESY report 83-062 (1983).
26. Reports by J. Johnson and R. Schwitters, Workshop on Electron Storage Ring Polarization, DESY M-82/09 (1982).

27. J. Kewisch, DESY report 83-032 (1983).

28. A. M. Kondratenko, Sov. Phys. JETP 39, 592 (1974).

29. K. Steffen, Ref. 26.

30. J. Buon, Orsay report LAL/RT/83-04 (1983), also talk presented in the 12th Int. Conf. High Energy Accel., Fermi Lab., 1983.

31. K. Steffen, DESY notes HERA-83/09 and HERA-83/16 (1983), unpublished.

32. Reports by K. Steffen, R. Rossmanith, Y. Yokoya, S. Holmes, J. Buon and A. Chao, Ref. 26.

33. R. Schmidt, Ref. 26. Also, D. Barber and H. Mais, this conference.